Geotextiles and Geomembranes xxx (2015) 1–10

Contents lists available at ScienceDirect

Geotextiles and Geomembranes

journal homepage: www.elsevier.com/locate/geotexmem

Characterization of geogrid reinforced ballast behavior at different levels of degradation through triaxial shear strength test and discrete element modeling

Yu Qian [a, *], Debakanta Mishra [b, 1, 2], Erol Tutumluer [a, 3], Hasan A. Kazmee [a, 4]

[a] Department of Civil and Environmental Engineering, The University of Illinois, Urbana-Champaign, Urbana, IL 61801, USA
[b] Department of Civil Engineering, Boise State University, Boise, ID 83725, USA

ARTICLE INFO

Article history:
Received 24 October 2014
Received in revised form
4 February 2015
Accepted 19 April 2015
Available online xxx

Keywords:
Geosynthetics
Railroad ballast
Geogrid
Triaxial testing
Discrete element method
Degradation

ABSTRACT

Recent research efforts at the University of Illinois have aimed at studying geogrid applications in railroad track structures, specifically focusing on ballast and subballast reinforcement. Ballast, typically comprising large sized aggregate particles with uniform gradation, is an essential layer in the railroad track substructure to facilitate load distribution and drainage. The primary mechanism of load transfer within the ballast layer involves inter-particle contact between ballast particles. Similarly, the effectiveness of ballast reinforcement with geogrids is primarily governed by the geogrid-aggregate interlock. Such interaction and the effectiveness thereof can change significantly as the level of grain size and shape degradation or fouling increases in the ballast layer with accumulation of train traffic. Although several studies in the past have investigated the effects of geogrid reinforcement on ballast shear strength and permanent deformation behavior, the effectiveness of geogrid reinforcement at different levels of ballast degradation needs to be further understood. In this study, monotonic triaxial shear strength tests were conducted on both new and degraded ballast materials with and without geogrid reinforcement. Two geogrid types, with square- and triangular-shaped apertures, were used in the laboratory to calibrate an aggregate imaging-based Discrete Element Method (DEM) modeling approach, which is capable of creating actual ballast aggregate particles as three-dimensional polyhedron blocks having the same particle size distributions and imaging quantified average shapes and angularities. The DEM model was observed to adequately capture the shear strength behavior of geogrid-reinforced triaxial ballast specimens prepared using both new and degraded ballast samples.

1. Introduction

Geogrids have been successfully used in railroad applications to construct railroad track over weak subgrades as well as reinforce ballast layer for improved lateral stability and reduced track settlement. For subgrade stabilization, the geogrids are often placed at the bottom of subballast and on top of the subgrade. Ballast reinforcement benefit of using geogrids is realized by limiting the lateral movement of aggregate particles. For this purpose, the geogrids are commonly installed at the ballast–subballast interface. The degree of interlocking to be maximized between geogrids and ballast particles is governed by several factors acting in combination, e.g., aggregate size and shape properties, geogrid types and properties (such as apertures, shapes and sizes of ribs, etc.), compactive effort during installation, and loading conditions.

The benefits of geogrid reinforcement have been highlighted by several laboratory research efforts, numerical simulations, as well as field implementation programs (Bathurst and Raymond, 1987; Raymond and Ismail, 2003; Indraratna et al., 2006; McDowell et al., 2006; Brown et al., 2007; Tutumluer et al., 2009; Qian et al., 2011, 2013a; Chen et al., 2012; Qian et al., 2013a,b; Mishra et al., 2014). These previous research studies have also identified subgrade conditions, number of geogrid layers, geogrid installation

* Corresponding author. Tel.: +1 2177994558; fax: +1 2173339464.
E-mail addresses: yuqian1@illinois.edu (Y. Qian), debmishra@boisestate.edu (D. Mishra), tutumlue@illinois.edu (E. Tutumluer), kazmee2@illinois.edu (H.A. Kazmee).
[1] Formerly Post-Doctoral Research Associate at the University of Illinois at Urbana-Champaign, USA.
[2] Tel.:+1 2084263710; fax: +1 2084262351.
[3] Tel.: +1 2173338637; fax: +1 2173331924.
[4] Tel.: +1 2174199971.

http://dx.doi.org/10.1016/j.geotexmem.2015.04.012
0266-1144/

depth, presence of moisture, aggregate size to geogrid aperture size ratio, geogrid aperture shape, etc. to be important controlling factors as far as geogrid reinforcement of railroad ballast is concerned. However, most of the current findings reported in the literature primarily focus on the performances of relatively new track sections where clean ballast with not much degradation was used in the beginning of its service life.

With the accumulation of tonnage in the field, ballast layers are progressively "fouled" with finer materials filling the void space within the coarse particle matrix. Although subgrade intrusion as well as spillage of foreign materials such as coal dust can contribute to the fouling phenomenon, degradation of ballast particles has been reported to contribute up to 76% of the total ballast layer fouling (Selig and Waters, 1994). The gradual filling up of voids in a ballast matrix due to particle degradation has been schematically represented in Fig. 1. Note that gradual degradation of ballast particles leads to considerable changes in the aggregate size and shape properties as well as ballast packing. Moreover, increasing degrees of fouling has the potential to significantly affect geogrid-aggregate interlock mechanisms. Such effects of ballast degradation on ballast strength and aggregate-geogrid interlock have not been thoroughly studied.

This paper describes preliminary findings from an ongoing research study at the University of Illinois focusing on triaxial testing of geogrid-reinforced ballast specimens using a large-scale triaxial test device and modeling the micromechanical interactions of geogrid-aggregate systems using the Discrete Element Method (DEM). Cylindrical triaxial specimens were prepared using new as well as degraded ballast materials reinforced with geogrids having either triangular or square shaped apertures. Monotonic triaxial shear strength tests were conducted to evaluate the reinforcement benefits through improved stress-strain behavior and shear strength properties. Unreinforced ballast specimens were also tested to serve as the control sets during this study. To simulate the triaxial tests and investigate geogrid reinforcement mechanisms, a numerical modeling approach based on the DEM was adopted with the capability to create actual ballast aggregate particles as three-dimensional polyhedron elements having the same particle size distributions and imaging quantified average shapes and angularities. Both the laboratory triaxial strength tests and the DEM simulation results are presented in this paper to evaluate the reinforcement benefits and mechanisms governing behavior of the ballast specimens reinforced with different geogrid types.

Fig. 2. Triaxial shear strength test setup.

2. Triaxial test device

A large-scale triaxial test device (The University of Illinois Ballast Triaxial Tester or TX-24) was recently developed at the University of Illinois for testing ballast size aggregate materials (Mishra et al., 2013). The test specimen dimensions are 305 mm (12 in.) in diameter and 610 mm (24 in.) in height. An internal load cell (Honeywell Model 3174) with a capacity of 89 kN (20 kips) placed on top of the specimen top platen measures accurately the applied load levels. Three vertical Linear Variable Differential Transformers (LVDTs) are mounted on the cylindrical test specimen at 120-degree angles to measure the vertical deformations of the specimen from three different side locations. Another LVDT is mounted on a circumferential chain wrapped around the specimen at the mid-height to measure the radial deformation of the test specimen. Fig. 2 shows a photograph of the TX-24 setup having an instrumented ballast specimen ready for shear strength testing.

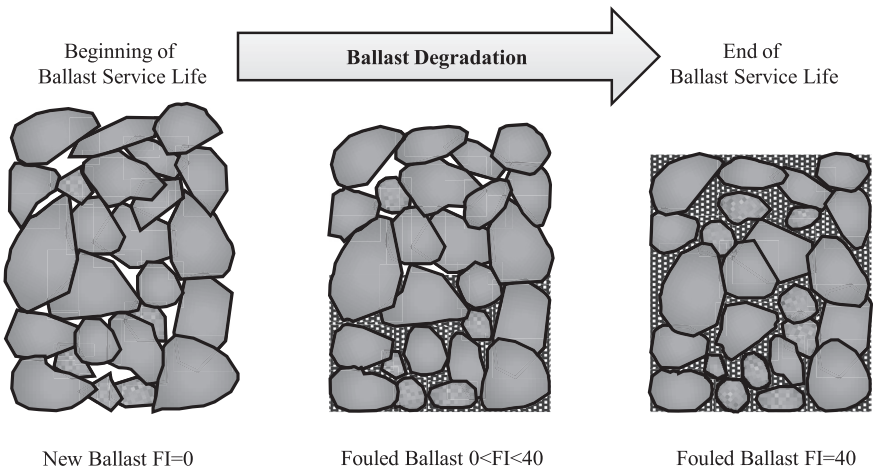

Fig. 1. Schematic drawing of ballast degradation (FI: Fouling Index).

Please cite this article in press as: Qian, Y., et al., Characterization of geogrid reinforced ballast behavior at different levels of degradation through triaxial shear strength test and discrete element modeling, Geotextiles and Geomembranes (2015), http://dx.doi.org/10.1016/j.geotexmem.2015.04.012

To adequately simulate the high loading rates associated with train movements, ballast specimens in this study were tested for shear strength properties by imposing a rapidly applied axial strain at a rate of 5% per second under a constant all-around confining pressure level of 138 kPa (20 psi) (Qian et al., 2013c). Considering the 610-mm (24-in.) high ballast specimens, such a loading rate corresponds to vertical ram movements of 30.5 mm (1.2 in.) per second. As such large movements of the loading ram are likely to cause instant bulging and shearing of the ballast specimens, the LVDTs were not mounted directly on the specimen during the shear strength testing. Accordingly, axial deformations of the specimens were recorded directly from the internal LVDT within the hydraulic actuator.

3. Ballast materials and geogrids

The ballast material used in this study comprised 100% crushed limestone aggregates, and was tested under oven-dried conditions. Degradation of ballast under train loading was simulated through Los Angeles (LA) abrasion testing of the new limestone ballast. A 10-kg representative sample (in terms of gradation and shape properties) of oven-dried clean new ballast was subjected to LA abrasion testing for 1500 turns to generate the material representing "fully fouled" conditions. Note that the extent of degradation achieved after 1500 LA abrasion cycle corresponded to a Fouling Index (FI, defined as the sum of percent by weight of material passing the 4.75 mm and 0.075 mm sieve sizes) of 40. Such a value of FI has been established to correspond to a heavily fouled or degraded ballast condition requiring immediate track maintenance activities (Selig and Waters, 1994). The degraded ballast materials thus generated were collected for conducting the triaxial shear strength tests and labeled as "Degraded Materials with Fines." Subsequently, all particles finer than 9.5 mm (3/8 in.) were removed from the degraded materials, and the resulting material (with all particles coarser than 9.5 mm or 3/8 in.) was labeled as "Degraded Ballast without Fines." In the context of this paper, the term "Fines" refers to all particles finer than 9.5 mm or passing the 3/8-in. sieve size. Such laboratory degradation effort of the ballast material inside the LA abrasion drum was repeated until sufficient amount of degraded ballast material was generated to prepare the triaxial test specimens. More details on the steps followed to obtain the degraded ballast through the LA abrasion testing have been provided elsewhere (Qian et al., 2014). Fig. 3 shows the grain size distributions of the new ballast material confirming to the US AREMA (American Railway Engineering and Maintenance of Way Association) No. 24 gradation requirements, along with the gradation curves for the degraded ballast material with and without fines.

It is important to note that although the importance of ballast gradation in governing the load carrying and drainage functionalities of ballast layers is widely recognized establishing direct links between gradation information and mechanisms governing ballast layer structural characteristics and drainage behavior is not trivial. Accordingly, to investigate particle contact and particle packing characteristics before and after degradation, approximately 10 kg each of the new and degraded (after 1500 turns in the LA abrasion drum) ballast materials were placed in an acrylic chamber with dimensions of 254 mm (10.0 in.) in diameter and 254 mm (10.0 in.) in height. Fig. 4 shows photographs of the side and top views of the acrylic chamber filled with ballast under the three conditions represented in Fig. 3. Photographs of the degraded ballast without fines are also included in Fig. 4 for comparison purposes. It is clearly seen that after 1500 turns, the same weight (about 10 kg) of degraded ballast occupied less volume compared to the new ballast in the acrylic chamber. However, for the same weight of degraded ballast, the specimen height remained nearly the same with or without fine particles as shown in Fig. 4. Accordingly, fines generated during the degradation process occupied the voids created by the large particles (particle sizes larger than 9.5 mm or 3/8 in.). At a degradation level corresponding to FI = 40, nearly all the voids created by the large particles were filled with fines.

Beside the grain size distribution, imaging based aggregate shape properties, i.e., the flat and elongated (F&E) ratio, the angularity index (AI), and the surface texture (ST) index, are key indices affecting railroad ballast performance and can be quantified by the University of Illinois Aggregate Image Analyzer (UIAIA) (Rao et al., 2002; Pan et al., 2006). The new and degraded ballast materials generated from the LA abrasion test in this study were scanned using the recently enhanced UIAIA or E-UIAIA, which utilizes three high resolution progressive scan type color cameras and the improved color thresholding (E-UIAIA) technique. The imaging-based morphological indices (F&E ratio, AI, and ST index)

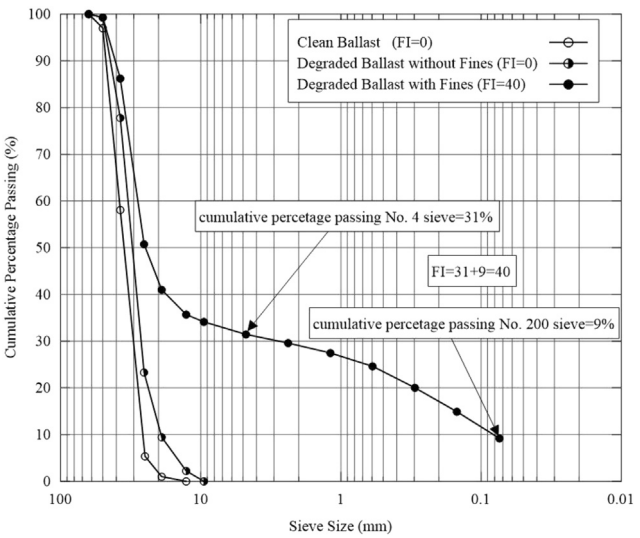

Fig. 3. Particle size distributions of clean and degraded ballast aggregates.

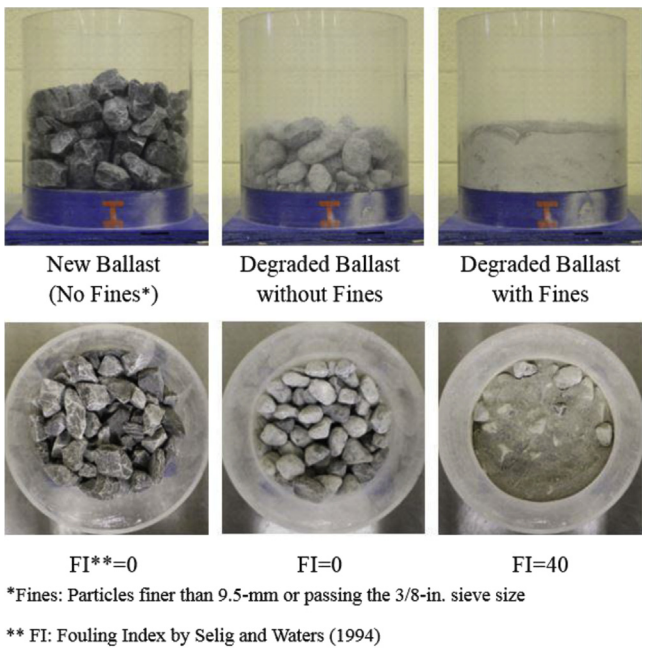

Fig. 4. Photos of side and top views of new and degraded aggregate packing.

Please cite this article in press as: Qian, Y., et al., Characterization of geogrid reinforced ballast behavior at different levels of degradation through triaxial shear strength test and discrete element modeling, Geotextiles and Geomembranes (2015), http://dx.doi.org/10.1016/j.geotexmem.2015.04.012

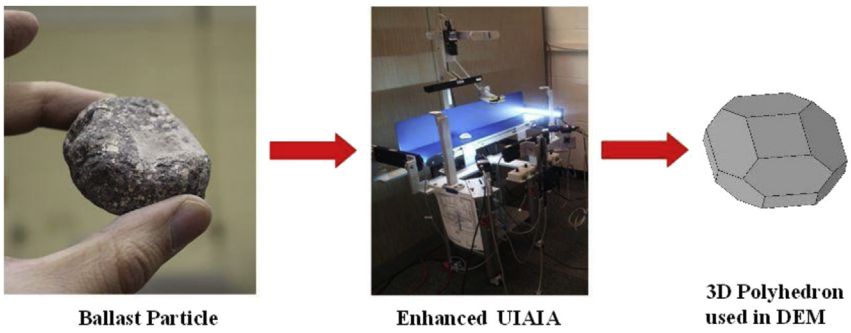

Fig. 5. Conceptual approach for aggregate imaging-based railroad ballast particle generation for discrete element method (DEM) simulations.

Table 1
Triaxial test specimen details and shape properties of large–sized (above 9.5-mm or 3/8-in.) particles.

	New ballast	Degraded ballast without fines	Degraded ballast with fines
Average Angularity Index (AI in degrees)	440	278	278
Average Flat & Elongated (F&E) Ratio	2.3	1.9	1.9
Average Surface Texture (ST) Index	1	1.3	1.3
Coefficient of Uniformity (C_u)	1.46	1.79	350
Coefficient of Curvature (C_c)	0.97	1.13	4.02
Specimen height	610 mm	610 mm	610 mm
Specimen diameter	305 mm	305 mm	305 mm
Specimen weight	70 kg	73 kg	94 kg
Compaction time	16 s	16 s	16 s
Void ratio (e)	0.68	0.61	0.25

were then established to generate ballast aggregate particle shapes as three-dimensional (3D) polyhedrons utilized in the ballast DEM model (see Fig. 5). Note that particles finer than 9.5 mm were not scanned using the E-UIAIA since these small sized particles were not created as 3D polyhedron elements in the elements in the DEM simulations. Accordingly, shape properties of different ballast materials discussed in this paper correspond to the averaged values of particles larger than 9.5 mm (3/8 in). Table 1 lists a summary of the E-UIAIA determined imaging-based morphological indices and certain gradation parameters of the ballast materials studied.

Each ballast sample studied (approximately 70 kg for new ballast, 73 kg for degraded ballast without fines, and 94 kg for degraded ballast with fines) was poured into an aluminum split mold in four lifts, and each lift was compacted using a 27.2-kg (60-lb.) electric jack hammer for 4 s (16 s in total). After compaction of the first two lifts, one layer of geogrid was placed carefully in the middle of the test specimen for making a geogrid reinforced ballast sample. When compaction of all four lifts was completed, each test specimen was checked for the total height and leveling of the top plate. The specimen void ratios computed were 0.68 for new ballast, 0.61 for degraded ballast without fines, and 0.25 for degraded ballast with fines. Fig. 6 shows photographs of the geogrids used in the current study, and the relevant properties of the geogrids are listed in Table 2.

4. DEM simulations of triaxial shear strength tests

Several recent research studies have reported successful applications of the Discrete Element Method (DEM) for simulating railroad ballast behavior (Indraratna et al., 2010; Lu and McDowell, 2010; Chen et al., 2012; Tutumluer et al., 2013). The DEM simulation approach developed at the University of Illinois (Ghaboussi and Barbosa, 1990; Zhao et al., 2006; Nezami et al., 2007) adopts real polyhedral particles and has the capability to create actual ballast aggregate particle shapes as 3D polyhedron elements having the same particle size distributions and imaging-quantified average shapes and angularities. This DEM approach was calibrated by the laboratory large scale direct shear test results (Tutumluer et al., 2006), validated by field track settlement predictions (Tutumluer et al., 2013), and has been successfully utilized to simulate complex ballast behavior, especially large scale triaxial tests with or

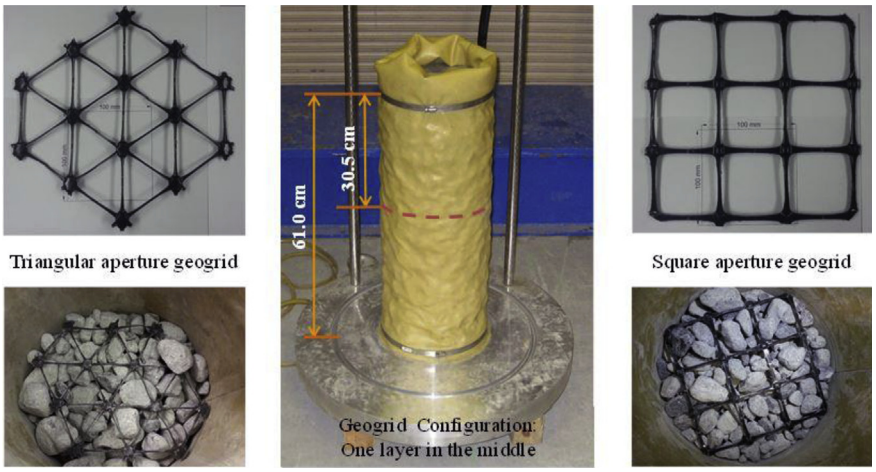

Fig. 6. Triangular and square aperture geogrids used in creating triaxial test specimens.

Please cite this article in press as: Qian, Y., et al., Characterization of geogrid reinforced ballast behavior at different levels of degradation through triaxial shear strength test and discrete element modeling, Geotextiles and Geomembranes (2015), http://dx.doi.org/10.1016/j.geotexmem.2015.04.012

Table 2
Properties of geogrids used.

	Square aperture	Triangular aperture	
	Side	Longitudinal	Diagonal
Aperture Dimensions (mm)	65	60	60
Ultimate QC Strength (kN/m)	30		
Junction Efficiency (percentage)		93	
Radial Stiffness (kN/m@0.5% strain)		350	

Table 3
Model parameters used in ballast DEM triaxial test simulations.

DEM Model Parameter	Value
Inter-particle Friction Angle	31°
Normal Contact Stiffness	20 MN/m
Shear Contact Stiffness	10 MN/m
Global Damping	0.06
Contact Damping	0.03
Time Step	2.70×10^{-6} s

without geogrid reinforcement (Qian et al., 2013a,b,c; Mishra et al., 2014).

Lee et al. (2012) used rigid rectangular cuboid discrete elements positioned in a cylindrical arrangement to simulate a flexible membrane and followed an "incremental displacement shearing method" to simulate triaxial shear strength tests of sand using the BLOKS3D DEM program. Similarly, the BLOKS3D code has been used by Qian et al. (2013c) to simulate large-scale triaxial shear strength tests of ballast materials, as well as in this study to simulate large-scale triaxial shear strength tests of degraded ballast materials with geogrid reinforcement. Fig. 7 provides an overview of the BLOKS3D DEM model and corresponding modeling parameters are listed in Table 3. Details of simulating a flexible membrane of the cylindrical test specimen by rigid discrete elements and application of "incremental displacement shearing method" in triaxial strength test simulation are provided elsewhere (Qian et al., 2013c). With the "incremental displacement" shearing method, the CPU time required to complete the triaxial shear strength simulations using a standard quad-core PC was approximately 30 h for the new ballast material, and slightly longer for degraded ballast without fines. Note that for specimens prepared using the degraded ballast material with fines, it was not possible to collect particle shape properties for the fine particles for constituting the triaxial specimen within the DEM environment. Moreover, the inclusion of numerous fine particles in the model would dramatically increase the computational expense, with the estimated CPU time to complete one simulation being in hundreds of days. Accordingly, the DEM simulations of triaxial shear strength tests performed under the scope of the current study were only limited to specimens prepared with new ballast and degraded ballast without fines.

After first establishing the membrane elements, approximately 500 particles, having the same gradation and shape properties of the actual limestone ballast material, were poured into the cylinder in two different sets. In between, a sheet of geogrid element was generated corresponding to the different reinforcement conditions being simulated. The geogrid element was modeled as a rigid non-deformable element with the same aperture dimensions as the geogrids used in experimental study. However, note that the rib thickness of the square aperture geogrid could not be accurately modeled using the DEM approach. This was because the rib thickness for the square aperture geogrid was significantly smaller than the individual ballast particle sizes. Modeling the exact rib dimensions of the square aperture geogrid would significantly increase the required computational effort. The rib thickness for the square aperture geogrid was therefore modeled in the current study as equal to that for the triangular aperture geogrid. Accordingly, the DEM simulated results for specimens with the square aperture geogrids are likely to overestimate the deviator stress values compared to the laboratory test results owing to the relatively thicker rib thicknesses.

5. Laboratory tests and DEM simulation results

Fig. 8 presents results from large-scale triaxial shear strength tests conducted on the new and degraded limestone specimens for up to 10% axial strain. Peak deviator stress values for the different ballast materials obtained from laboratory experiments and DEM simulations are listed in Table 4. As shown in Fig. 8, all specimens exhibited similar stress-strain behavior under small magnitudes of imposed axial strains. This was primarily because under small imposed axial strain and corresponding small radial bulging conditions, the aggregate-geogrid interlock mechanism is not fully mobilized. However upon gradual increase in the axial strain levels,

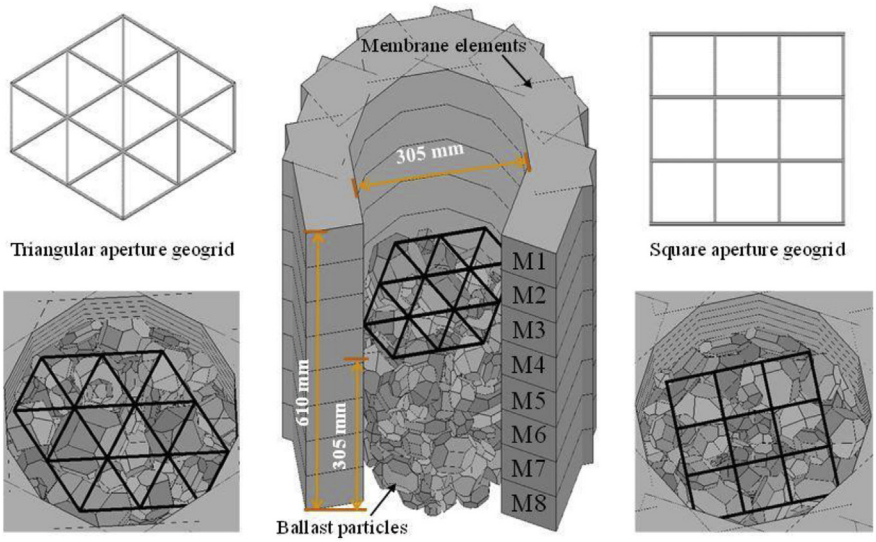

Fig. 7. Geogrids and triaxial ballast specimen established in DEM simulations.

Please cite this article in press as: Qian, Y., et al., Characterization of geogrid reinforced ballast behavior at different levels of degradation through triaxial shear strength test and discrete element modeling, Geotextiles and Geomembranes (2015), http://dx.doi.org/10.1016/j.geotexmem.2015.04.012

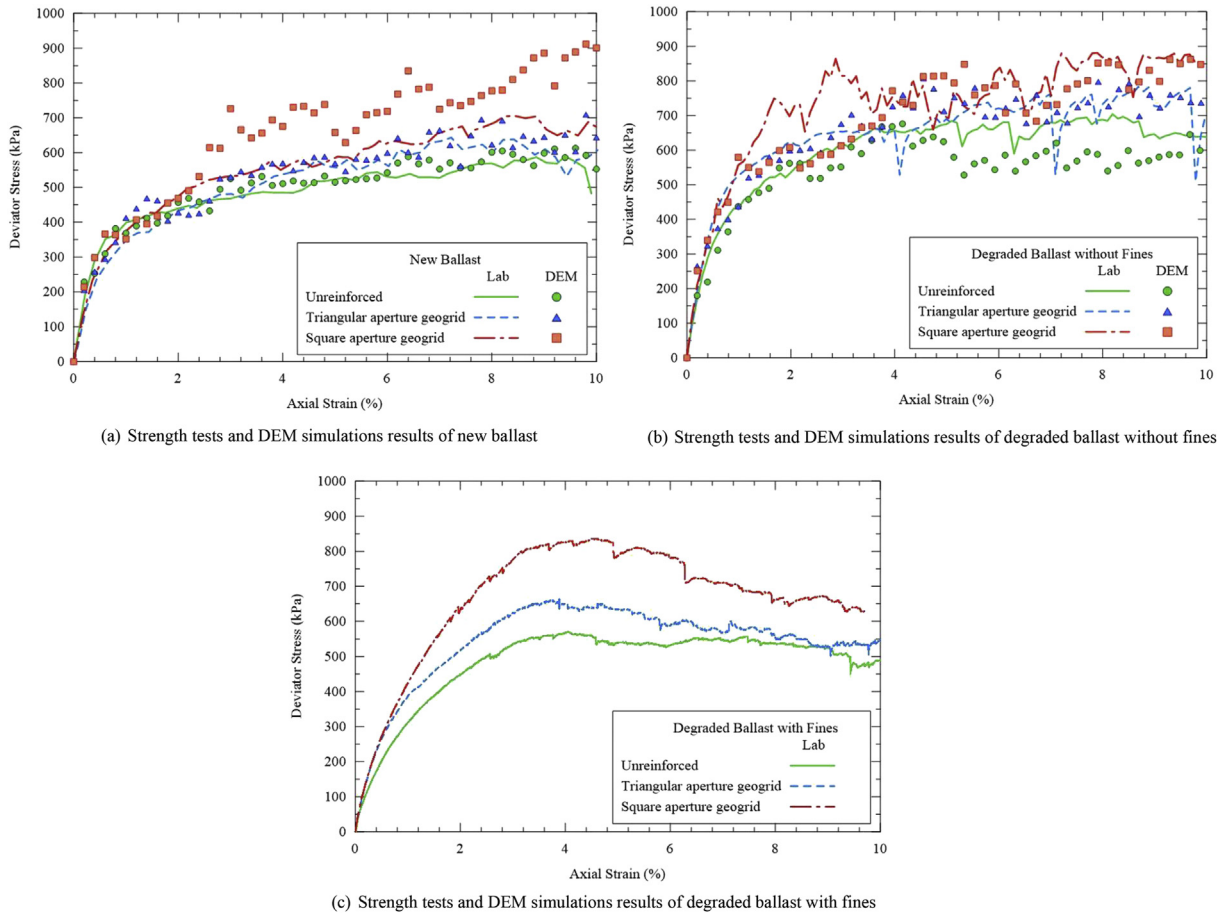

(a) Strength tests and DEM simulations results of new ballast

(b) Strength tests and DEM simulations results of degraded ballast without fines

(c) Strength tests and DEM simulations results of degraded ballast with fines

Fig. 8. Laboratory triaxial ballast strength tests and DEM simulation results (Note that only laboratory data presented for the Degraded Ballast Material with Fines).

Table 4
Peak strength values from laboratory tests and DEM simulation predictions.

	Ballast type	Unreinforced (kPa)	Triangular aperture geogrid reinforced (kPa)	Square aperture geogrid reinforced (kPa)
Lab	Clean	590	643	705
	Degraded w/o fines	709	786	894
	Degraded w/fines	570	664	836
DEM	Clean	604	709	912
	Degraded w/o fines	693	813	880

significant interlock between the geogrid and ballast particles is achieved to prevent lateral movements of particles and the corresponding radial bulging is prevented.

It is important to note that significant “jumps” in the stress-strain curve are observed at high axial strain levels. This can be attributed to the sudden breakage of geogrid ribs (often observed upon examining the geogrids after tests were completed in the laboratory), under excessive ballast-geogrid interaction forces or ballast particle breakage, and subsequent reorientation of individual ballast particles. As a certain geogrid rib or aggregate particle breaks, the adjacent ballast particles reorient themselves, and the system attains a new configuration with new interlocks formed between aggregate particles and the geogrid. This results in a restoration of the specimen shear strength until the next breakage of a geogrid rib occurs. The DEM simulation results presented in Fig. 8 showed generally good agreement with the experimental data. In some cases, the DEM simulations overestimated the strength of geogrid reinforced specimens; this is due to the fact that breakage of the geogrid ribs or aggregate particles was not allowed in the DEM simulations.

Another interesting phenomenon observed from both the experimental and DEM simulation results is that particle degradation did not result in significant strength loss for the ballast specimens when compared with the new ballast material. On the contrary, in most cases the degraded ballast with or without fines yielded higher strength than new ballast. Comparing the gradations of the three ballast materials used in this study (see Fig. 3), the degraded ballast without fines comprised higher number of smaller particles, and was more “well” graded compared to the new ballast material satisfying AREMA No. 24 uniform gradation specification. The smaller particles within the degraded ballast matrix can potentially help stabilize the aggregate skeleton, thus resulting in higher shear strength. Moreover, from the imaging-based shape properties listed in Table 1, the degraded ballast particles have significantly lower Angularity Index (AI), and tend to be more cubical and smoother and hence less susceptible to abrading of

Please cite this article in press as: Qian, Y., et al., Characterization of geogrid reinforced ballast behavior at different levels of degradation through triaxial shear strength test and discrete element modeling, Geotextiles and Geomembranes (2015), http://dx.doi.org/10.1016/j.geotexmem.2015.04.012

sharp corners and edges during strength testing when compared to the new ballast particles. Accordingly, more cubical degraded ballast particles with smoother surfaces can attain a denser packing configuration leading to higher densities for the specimens. This in turn results in higher peak deviator stress values achieved during shear strength testing. Note that a similar trend was reported by Tutumluer et al. (2013) when ballast with lower angularity yielded less settlement in the field due to better packing.

For the specimens prepared with the degraded ballast material with fines, most of fines (material finer than 9.5 mm or 3/8 in.) filled the void created by larger particles (see Fig. 4), thus helping to stabilize the aggregate skeleton. However, presence of excessive fines in the aggregate matrix results in the loss of contact between large particles, thus making it easier for the large particles to reorient and rearrange. This in-turn can lead to significant reductions in the specimen shear strength. The fine particles thus present stabilization and also lubrication effects in the specimens prepared with the degraded ballast material with fines. This was the reason that degraded ballast with fines had lower strength than degraded ballast without fines but higher strength than new ballast. This was also the reason that the degraded ballast with fines had much smoother stress-strain curves during strength tests. However, all the test results presented here were under dry conditions, which means no moisture was involved in the test specimens. Upon introduction of moisture into the specimens, the shear strength behavior of ballast under the three conditions tested in this study can be significantly different, and will be presented in future publications.

6. Effect of axial strain on specimen geometry change

The measurement of volumetric strain, and tracking the corresponding changes in specimen geometry during shear strength testing of large aggregate particles, such as railroad ballast, can be very challenging. As already mentioned, on-specimen deformation measurements using LVDTs was not carried out during the current study to prevent damage to the instrumentation upon instant excessive bulging of the specimen. However, information regarding volumetric strains and specimen geometric changes during triaxial shear strength testing of ballast can be easily extracted from numerical simulations. Changes in the radius of each membrane layer as well as specimen volume with imposed axial strain for all the test configurations are presented in Fig. 9. Corresponding information for new ballast was provided elsewhere (Mishra et al., 2014). Fig. 9 clearly shows that the initial radius of each membrane layer was identical (152.4 mm or 6 in.), but underwent different change patterns with gradual increases in axial strain. Note that membrane layer M8 behaved differently than other layers due to boundary effects (see Fig. 9). Changes in the membrane layer radius can be interpreted as bulging of the specimen at the corresponding locations. Membrane layers M4 through M7 exhibited the largest increase in radius for both reinforced as well as unreinforced cases. However, the largest radius was 175.6 mm (M6) for the unreinforced case; 171.6 mm (M5) for the triangular aperture geogrid reinforced case; and 167.0 mm (M6) for the square aperture geogrid reinforced case. From Fig. 9, the radius increases for geogrid-reinforced cases were more "uniform" compared to the unreinforced case. This is a

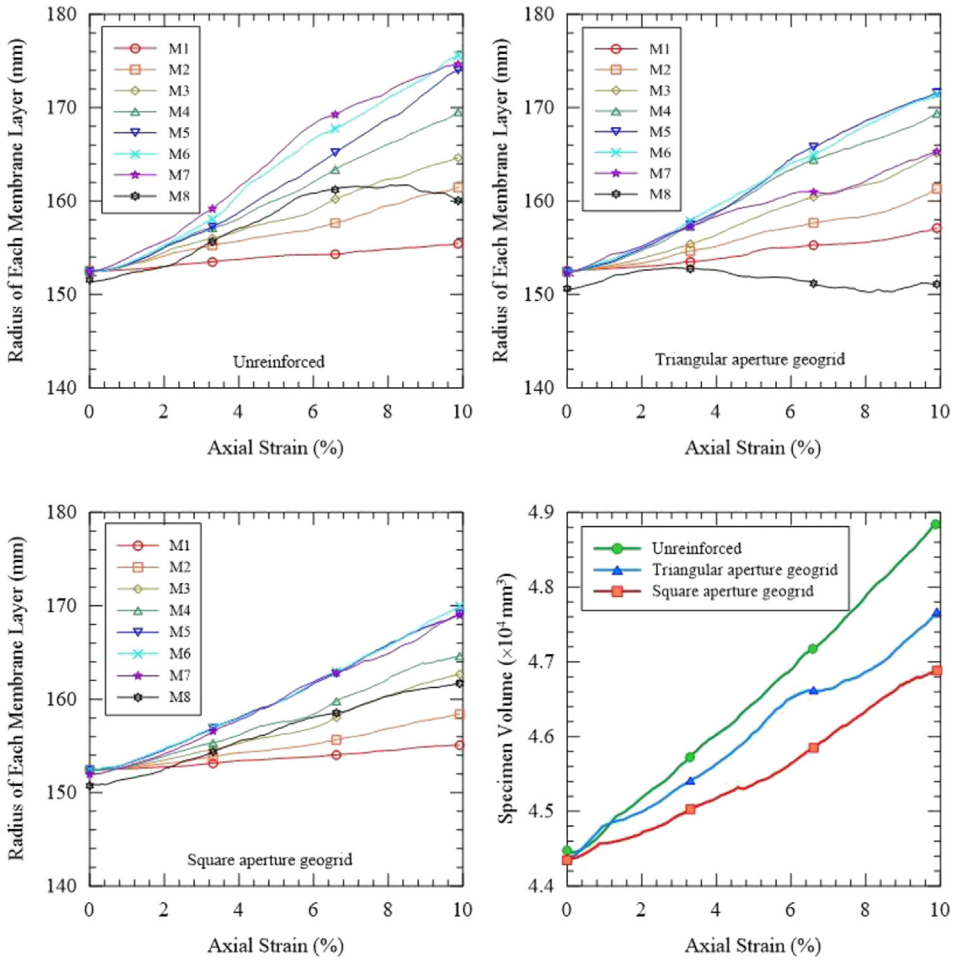

Fig. 9. Volume and radius of each membrane layer element in test specimens with degraded ballast without fines computed in DEM simulations.

Please cite this article in press as: Qian, Y., et al., Characterization of geogrid reinforced ballast behavior at different levels of degradation through triaxial shear strength test and discrete element modeling, Geotextiles and Geomembranes (2015), http://dx.doi.org/10.1016/j.geotexmem.2015.04.012

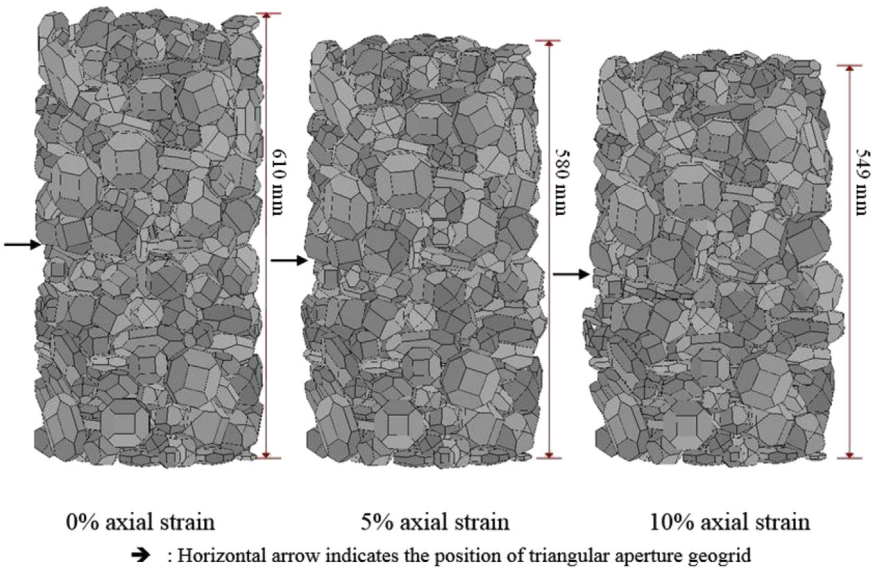

Fig. 10. Front view of DEM simulation of the triangular aperture geogrid reinforced specimen of the degraded ballast without fines.

direct manifestation of the "restraining" effect of geogrids against lateral movement. Note that for unreinforced specimens, particles near the specimen mid-depth underwent large lateral movements, with particles near top and bottom of specimen exhibiting no significant lateral movement. Fig. 9 also shows that gradual increase in the axial strain initially resulted in a small reduction in the specimen volume, followed by continued increase. The unreinforced specimen demonstrated the highest degree of dilation, whereas the dilation for the specimen with a square-aperture geogrid was the lowest. This is also indicative of the effectiveness of geogrids as far as restrained lateral particle movement during shear strength testing is concerned.

For better visualization of changes in specimen geometry with increasing axial strain levels, Fig. 10 shows the front view of a DEM-generated triaxial ballast specimen (degraded ballast without fines) reinforced with a triangular aperture geogrid at three different axial strain levels. As shown in the figure, the maximum bulging takes place slightly below the specimen mid-depth (location of geogrid placement), which corresponds to layers M5 and M6. This visual representation is in agreement with the trends in radius change reported in Fig. 9. Specimen configurations in DEM simulation and laboratory test under 10% strain are compared in Fig. 11.

Note that the particle reorientations at the ballast-geogrid interface can also have significant effects on the changes in specimen geometry with increasing axial strain levels. As an example, this can be illustrated considering two individual ballast particles from one of the DEM simulations. Fig. 12 shows two ballast particles (Particle A and Particle B) and their contacts with the geogrid

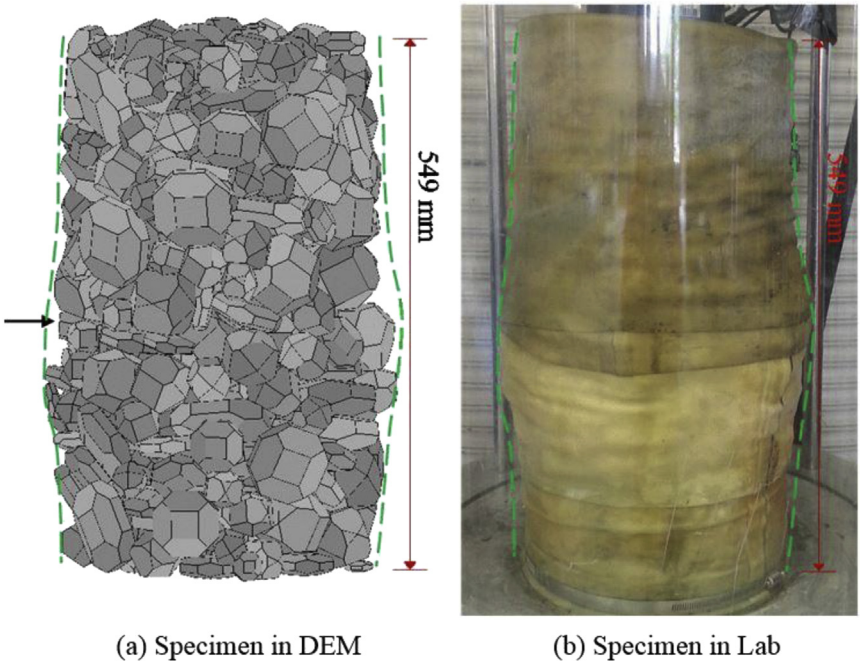

Fig. 11. Deformed ballast specimen configuration of the triangular aperture geogrid reinforced specimen of the degraded ballast without fines: (a) Laboratory test; (b) DEM simulation.

Please cite this article in press as: Qian, Y., et al., Characterization of geogrid reinforced ballast behavior at different levels of degradation through triaxial shear strength test and discrete element modeling, Geotextiles and Geomembranes (2015), http://dx.doi.org/10.1016/j.geotexmem.2015.04.012

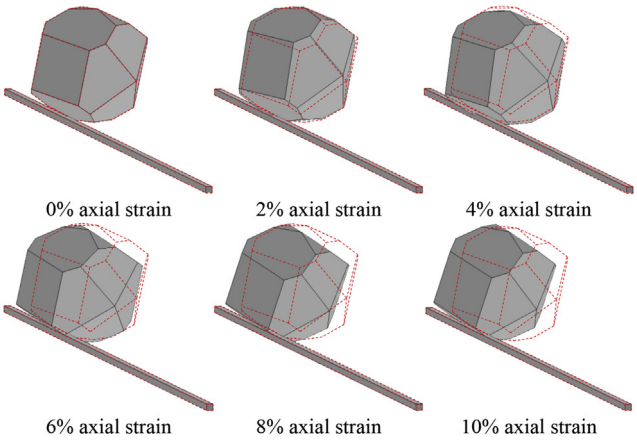

(a) Particle A and its contacts with geogrid element (red dash line indicates original position)

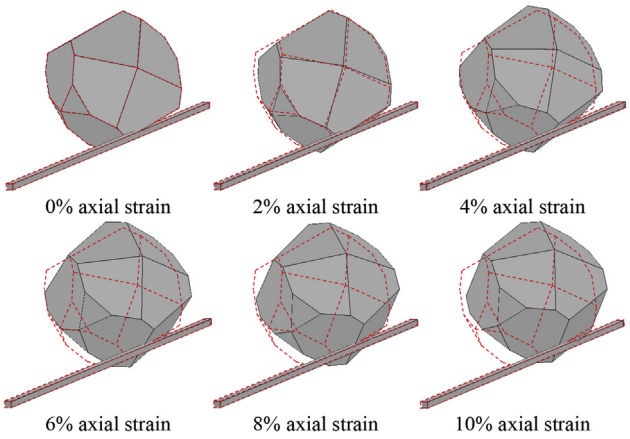

(b) Particle B and its contact with geogrid element (red dash line indicates original position)

Fig. 12. Two single particles analyzed and their contacts with geogrid element in DEM simulations of a shear strength test.

element from the DEM simulation. Although both the particles remained in contact with the geogrid element throughout the triaxial shear strength test simulation, the type of particle rotation and reorientation at the ballast-geogrid interface with increasing axial strain was different for the two. Particle A exhibited a potential trend to climb over the geogrid element, particularly at relatively large (~6%) axial strain levels. However, Particle B on the other hand, tended to come into the geogrid aperture throughout the shearing procedure. Such detailed information regarding contact behavior obtained from the DEM simulations can be potentially used to optimize the combination of particle shape, geogrid rib shape, particle size, and aperture size, etc., thus maximizing effective interlocking between geogrids and aggregate particles.

7. Summary and conclusions

This paper presented results of shear strength tests conducted on geogrid-reinforced railroad ballast specimens using a large-scale triaxial test device. Geogrids with triangular and square shape apertures were used to reinforce both new and degraded (with and without fine particles smaller than 9.5 mm) ballast specimens. Numerical simulations were performed using an aggregate image analysis-based Discrete Element Method (DEM) modeling approach to demonstrate its capabilities for studying geogrid-aggregate interlock reinforcement mechanisms. The following conclusions can be drawn from this study:

Both triangular and square-aperture geogrids were found to effectively increase the peak deviator stress values for triaxial specimens prepared using the new and degraded ballast materials. Highest shear strength values in the current study were obtained for ballast specimens reinforced using the square-aperture geogrid. However, it should be noted that the objective of this study was not to compare the performances of different geogrid types, but rather to demonstrate the capabilities of the DEM approach in simulating ballast reinforcement phenomenon. Accordingly, further research is required to fully investigate aperture shape effects on the overall geogrid reinforcement mechanism.

Specimens prepared using degraded ballast materials did not necessarily exhibit lower shear strength values compared to those prepared using the new ballast material under dry conditions. On the contrary, in most cases, specimens prepared using the degraded ballast materials exhibited higher shear strength values under dry conditions and similar loading and reinforcement conditions compared to those prepared using the new ballast material. Specimens prepared with the degraded ballast material without fines yielded the highest shear strength values under both unreinforced as well as geogrid-reinforced configurations.

The aggregate imaging-based DEM simulation platform developed at the University of Illinois could adequately simulate the stress-strain behavior of both unreinforced and geogrid-reinforced ballast specimens under monotonic triaxial shear strength tests. Some important information such as volumetric change and geometry change due to specimen bulging, that are difficult to measure in the laboratory during triaxial shear strength tests, can be easily extracted from DEM simulations. The DEM approach also proved to be adequate in capturing contact behavior details at the geogrid-aggregate interfaces. This aggregate imaging based DEM simulation platform currently being further developed at the University of Illinois has the potential to quantify individual effects of various geogrid properties, such as aperture shape and size and rib dimensions, on the aggregate assembly.

Acknowledgments

This research was partially supported by the Geosynthetics Institute (GSI) Fellowship. All geogrids used in this study were provided by Tensar International, Inc. Huseyin Boler, PhD student at the University of Illinois, provided considerable help during LA abrasion testing. Maziar Moaveni and Wenting Hou, also PhD students at the University of Illinois, helped operate the E-UIAIA aggregate image analyzer equipment and scanned ballast particles. The Illinois Center for Transportation (ICT) provided laboratory space for operation of the TX-24 test setup. All the support and help are greatly appreciated. The opinions expressed in this article are solely those of the authors and do not represent the opinions of the funding agency.

References

Bathurst, R.J., Raymond, G.P., 1987. Geogrid reinforcement of ballasted track. Transp. Res. Rec. 1153, 8–14.

Brown, S.F., Kwan, J., Thom, N.H., 2007. Identifying the key parameters that influence geogrid reinforcement of railway ballast. Geotext. Geomembr. 25 (6), 326–335.

Chen, C., McDowell, G.R., Thom, N.H., 2012. Discrete element modeling of cyclic loads of geogrid-reinforced ballast under confined and unconfined condition. Geotext. Geomembr. 35 (12), 76–86.

Please cite this article in press as: Qian, Y., et al., Characterization of geogrid reinforced ballast behavior at different levels of degradation through triaxial shear strength test and discrete element modeling, Geotextiles and Geomembranes (2015), http://dx.doi.org/10.1016/j.geotexmem.2015.04.012

Ghaboussi, J., Barbosa, R., 1990. Three dimensional discrete element method for granular materials. Int. J. Numer. Anal. Methods Geomech. 14, 451–472.
Indraratna, B., Khabbaz, H., Salim, W., Christie, D., 2006. Geotechnical properties of ballast and the role of geosynthetics in rail track stabilization. J. Ground Improv. 10 (3), 91–102.
Indraratna, B., Thakur, P.K., Vinod, J.S., 2010. Experimental and numerical study of railway ballast behavior under cyclic loading. Int. J. Geomech. ASCE 10 (4), 136–144.
Lee, S.J., Hashash, Y.M.A., Nezami, E.G., 2012. Simulation of triaxial compression test with polyhedral discrete elements. Comput. Geotech. 43, 92–100.
Lu, M., McDowell, G.R., 2010. Discrete element modelling of railway ballast under monotonic and cyclic triaxial loading. Geotechnique 60 (6), 459–467.
McDowell, G.R., Harireche, O., Konietzky, H., Brown, S.F., Thom, N.H., 2006. Discrete element modelling of geogrid-reinforced aggregates. In: Proceedings of the Institution of Civil Engineers—Geotechnical Engineering, 159, pp. 35–48.
Mishra, D., Kazmee, H., Tutumluer, E., Pforr, J., Read, D., Gehringer, E., 2013. Characterization of railroad ballast behavior under repeated loading: results from new large triaxial test setup. Transp. Res. Rec. J. Transp. Res. Board 2374, 169–179. Transportation Research Board of the National Academies, Washington, D.C.
Mishra, D., Qian, Y., Kazmee, H., Tutumluer, E., 2014. Investigation of geogrid-reinforced railroad ballast behavior using large-scale triaxial testing and discrete element modeling. Transp. Res. Rec. J. Transp. Res. Board (2462), 98–108. Transportation Research Board of the National Academies, Washington, D.C.
Nezami, E.G., Hashash, Y.M.A., Zhao, D., Ghaboussi, J., 2007. Simulation of front end loader bucket-soil interaction using discrete element method. Int. J. Numer. Anal. Methods Geomech. 31 (9), 1147–1162.
Pan, T., Tutumluer, E., Carpenter, S.H., 2006. Effect of coarse aggregate morphology on permanent deformation behavior of Hot Mix Asphalt. J. Transp. Eng. 132 (7), 580–589.
Qian, Y., Tutumluer, E., Huang, H., 2011. A validated discrete element modeling approach for studying geogrid-aggregate reinforcement mechanisms. In: GeoFrontiers 2011, ASCE Geo-Institute. March 13-16, Dallas, TX.
Qian, Y., Mishra, D., Tutumluer, E., Kwon, J., 2013a. Comparative evaluation of different aperture geogrids for ballast reinforcement through triaxial testing and discrete element modeling. In: Geosynthetics 2013. April 1–4, Long Beach, CA.
Qian, Y., Mishra, D., Tutumluer, E., Kwon, J., 2013b. Discrete element modeling of ballast reinforced with triangular aperture geogrid. In: 9th International Conference on Bearing Capacity of Roads, Railways and Airfields. June 25–27, Trondheim, Norway.
Qian, Y., Lee, S.J., Tutumluer, E., Hashash, Y.M.A., Mishra, D., Ghaboussi, J., 2013c. Discrete element method for simulating ballast shear strength from large scale triaxial tests. J. Transp. Res. Board 2374, 126–135. Transportation Research Board of the National Academies, Washington, D.C.
Qian, Y., Boler, H., Moaveni, M., Tutumluer, E., Hashash, Y.M.A., Ghaboussi, J., 2014. Characterizing ballast degradation through Los Angeles abrasion test and image analysis. Transp. Res. Rec. J. Transp. Res. Board 2448, 142–151. Transportation Research Board of the National Academies, Washington, D.C.
Rao, C., Tutumluer, E., Kim, I.T., 2002. Quantification of coarse aggregate angularity based on image analysis. Transp. Res. Rec. 1787, 193–201.
Raymond, G., Ismail, I., 2003. The effect of geogrid reinforcement on unbound aggregates. Geotext. Geomembr. 21 (6), 355–380.
Selig, E.T., Waters, J.M., 1994. Track Geotechnology and Substructure Management. Thomas Telford, Ltd.
Tutumluer, E., Huang, H., Hashash, Y.M.A., Ghaboussi, J., 2006. Aggregate shape effects on ballast tamping and railroad track lateral stability. In: Proceedings of the AREMA Annual Conference, Louisville, Kentucky, USA, September 17–20.
Tutumluer, E., Huang, H., Bian, X., 2009. Research on the behavior of geogrids in stabilization applications. In: Proc., Jubilee Symposium on Polymer Geogrid Reinforcement, September 8, 2009, London, UK.
Tutumluer, E., Qian, Y., Hashash, Y.M.A., Ghaboussi, J., Davis, D., 2013. Discrete element modeling of ballasted track deformation behavior. Int. J. Rail Transp. 1 (1–2), 57–73.
Zhao, D., Nezami, E.G., Hashash, Y.M.A., Ghaboussi, J., 2006. Three-dimensional discrete element simulation for granular materials. Eng. Comput. 23 (7), 749–770.

Please cite this article in press as: Qian, Y., et al., Characterization of geogrid reinforced ballast behavior at different levels of degradation through triaxial shear strength test and discrete element modeling, Geotextiles and Geomembranes (2015), http://dx.doi.org/10.1016/j.geotexmem.2015.04.012